Figure legends

Figure 1 Effects of ONO-4819 vs. risedronate on biomechanical strength

Thirty-three-week-old OVX rats were treated with ONO-4819, risedronate or their combination at the indicated doses (in μg/kg) for 11 weeks, and biomechanical strength was determined at the proximal tibiae by finite element analysis. Data are expressed as the mean +/- SEM (n=10 each). * $p<0.05$ vs. Sham group by Wilcoxon's rank sum test, # $p<0.05$ vs. OVX group by Steel's test, § $p<0.05$ vs. ONO-4819 (3 μg/kg) alone by the Steel test

Figure 2 Results of histomorphometric analysis

Thirty-three-week-old OVX rats were treated with ONO-4819, risedronate or their combination at the indicated doses (in μg/kg) for 11 weeks, and histomorphometric analysis was performed at the secondary spongiosa of the proximal tibial metaphysis. BFR: bone formation rate, Ob.S: osteoblast surface, MS: mineralizing surface, Oc.S: osteoclast surface. Data were corrected for bone surface (BS) and expressed as the mean +/- SEM (n=10 each). * $p<0.05$ vs. Sham group by Wilcoxon's rank sum test, # $p<0.05$ vs. OVX group (by Steel's test for comparison with ONO-4819-treated group and by Wilcoxon's rank sum test for comparison between risedoronate-treated and combined treatment groups.), ∫ $p<0.05$ vs. ONO-4819 (3 μg/kg) alone by Wilcoxon's rank sum test.

Figure 3 Effects of ONO-4819 vs. risedronate on formation/resorption ratio

Thirty-three-week-old OVX rats were treated with ONO-4819, risedronate or their combination at the indicated doses (in μg/kg) for 11 weeks, and histomorphometric analysis was performed at the secondary spongiosa of the proximal tibial metaphysis. As an index of net bone formation, the ratio of labeled surface to eroded surface was calculated. Data are expressed as the mean +/- SEM (n=10 each). $^{\#}p<0.05$ vs. OVX group (Steel's test was used for comparison with ONO-4819-treated groups; and Wilcoxon's rank sum test, for that between risedoronate-treated group and combined treatment group.).

References

1. Raisz LG. Prostaglandins and bone: physiology and pathophysiology. Osteoarthritis Cartilage 1999; **7**: 419-21.
2. Raisz LG, Sandberg AL, Goodson JM, Simmons HA, Mergenhagen SE. Complement-dependent stimulation of prostaglandin synthesis and bone resorption. Science 1974; **185:** 789-91.
3. Lin BY, Jee WS, Ma YF, Ke HZ, Kimmel DB, Li XJ. Effects of prostaglandin E2 and risedronate administration on cancellous bone in older female rats. Bone 1994; **15:** 489-96.
4. Jee WS, Ma YF. The in vivo anabolic actions of prostaglandins in bone. Bone 1997; **21:** 297-304.
5. Coleman RA, Smith WL, Narumiya S. International Union of Pharmacology classification of prostanoid receptors: properties, distribution, and structure of the receptors and their subtypes. Pharmacol Rev 1994; **46:** 205-29.
6. Miyaura C, Inada M, Suzawa T, Sugimoto Y, Ushikubi F, Ichikawa A, Narumiya S, Suda T. Impaired bone resorption to prostaglandin E2 in prostaglandin E receptor EP4-knockout mice. J Biol Chem 2000; **275:** 19819-23.
7. Suzawa T, Miyaura C, Inada M, Maruyama T, Sugimoto Y, Ushikubi F, Ichikawa A, Narumiya S, Suda T. The role of prostaglandin E receptor subtypes (EP1, EP2, EP3, and EP4) in bone resorption: an analysis using specific agonists for the respective EPs. Endocrinology 2000; **141:** 1554-9.
8. Yoshida K, Oida H, Kobayashi T, Maruyama T, Tanaka M, Katayama T, Yamaguchi K, Segi E, Tsuboyama T, Matsushita M, Ito K, Ito Y, Sugimoto Y, Ushikubi F, Ohuchida S, Kondo K, Nakamura T, Narumiya S. Stimulation of bone formation and prevention of bone loss by prostaglandin E EP4 receptor activation. Proc Natl Acad Sci U S A 2002; **99:** 4580-5.
9. Ruegsegger P, Koller B, Muller R. A microtomographic system for the nondestructive evaluation of bone architecture. Calcif Tissue Int 1996; **58:** 24-9.
10. Muller R, Hahn M, Vogel M, Delling G, Ruegsegger P. Morphometric analysis of noninvasively assessed bone biopsies: comparison of high-resolution computed tomography and histologic sections. Bone 1996; **18:** 215-20.

11. Ito M, Nishida A, Nakamura T, Uetani M, Hayashi K. Differences of three-dimensional trabecular microstructure in osteopenic rat models caused by ovariectomy and neurectomy. Bone 2002; **30:** 594-8.
12. Ito M, Nakamura T, Matsumoto T, Tsurusaki K, Hayashi K. Analysis of trabecular microarchitecture of human iliac bone using microcomputed tomography in patients with hip arthrosis with or without vertebral fracture. Bone 1998; **23:** 163-9.
13. Laib A, Hildebrand T, Hauselmann HJ, Ruegsegger P. Ridge number density: a new parameter for in vivo bone structure analysis. Bone 1997; **21:** 541-6.
14. Hildebrand T, Ruegsegger P. Quantification of bone microarchitecture with the structure model index. Comput Methods Biomech Biomed Engin 1997; **1:** 15-23.
15. Ulrich D, van Rietbergen B, Laib A, Ruegsegger P. The ability of three-dimensional structural indices to reflect mechanical aspects of trabecular bone. Bone 1999; **25:** 55-60.
16. Boyce RW, Ebert DC, Youngs TA, Paddock CL, Mosekilde L, Stevens ML, Gundersen HJ. Unbiased estimation of vertebral trabecular connectivity in calcium-restricted ovariectomized minipigs. Bone 1995; **16:** 637-42.
17. Odgaard A, Gundersen HJ, Quantification of connectivity in cancellous bone, with special emphasis on 3-D reconstructions. Bone 1993; **14:** 173-82.
18. van Rietbergen B, Weinans H, Huiskes R, Odgaard A. A new method to determine trabecular bone elastic properties and loading using micromechanical finite-element models. J Biomech 1995; **28:** 69-81.
19. Van Rietbergen B, Odgaard A, Kabel J, Huiskes R. Direct mechanics assessment of elastic symmetries and properties of trabecular bone architecture. J Biomech 1996; **29:** 1653-7.
20. Ito M, Nishida A, Aoyagi K, Uetani M, Hayashi K, Kawase M. Effects of risedronate on trabecular microstructure and biomechanical properties in ovariectomized rat tibia. Osteoporos Int 2005; **16:** 1042-8.
21. Burr DB, Hirano T, Turner CH, Hotchkiss C, Brommage R, Hock JM. Intermittently administered human parathyroid hormone(1-34) treatment increases intracortical bone turnover and porosity without reducing bone strength in the humerus of ovariectomized cynomolgus monkeys. J Bone Miner

Res 2001; **16:** 157-65.

22. Li X, Okada Y, Pilbeam CC, Lorenzo JA, Kennedy CR, Breyer RM, Raisz LG Knockout of the murine prostaglandin EP2 receptor impairs osteoclastogenesis in vitro. Endocrinology 2000; **141:** 2054-61.
23. Yasuda H, Shima N, Nakagawa N, Yamaguchi K, Kinosaki M, Mochizuki S, Tomoyasu A, Yano K, Goto M, Murakami A, Tsuda E, Morinaga T, Higashio K, Udagawa N, Takahashi N, Suda T. Osteoclast differentiation factor is a ligand for osteoprotegerin/osteoclastogenesis-inhibitory factor and is identical to TRANCE/RANKL. Proc Natl Acad Sci U S A 1998; **95:** 3597-602.
24. Ono K, Kaneko H, Choudhary S, Pilbeam CC, Lorenzo JA, Akatsu T, Kugai N, Raisz LG. Biphasic effect of prostaglandin E2 on osteoclast formation in spleen cell cultures: role of the EP2 receptor. J Bone Miner Res 2005; **20:** 23-9.
25. Tsujisawa T, Inoue H, Nishihara T. SC-19220, antagonist of prostaglandin E2 receptor EP1, inhibits osteoclastogenesis by RANKL. J Bone Miner Res 2005; **20:** 15-22.
26. Kobayashi Y, Take I, Yamashita T, Mizoguchi T, Ninomiya T, Hattori T, Kurihara S, Ozawa H, Udagawa N, Takahashi N. Prostaglandin E2 receptors EP2 and EP4 are down-regulated during differentiation of mouse osteoclasts from their precursors. J Biol Chem 2005; **280:** 24035-42.
27. Borah B, Dufresne TE, Chmielewski PA, Gross GJ, Prenger MC, Phipps RJ. Risedronate preserves trabecular architecture and increases bone strength in vertebra of ovariectomized minipigs as measured by three-dimensional microcomputed tomography. J Bone Miner Res 2002; **17:** 1139-47.
28. Black DM, Greenspan SL, Ensrud KE, Palermo L, McGowan JA, Lang TF, Garnero P, Bouxsein ML, Bilezikian JP, Rosen CJ. The effects of parathyroid hormone and alendronate alone or in combination in postmenopausal osteoporosis. N Engl J Med 2003; **349:** 1207-15.
29. Finkelstein JS, Hayes A, Hunzelman JL, Wyland JJ, Lee H, Neer RM. The effects of parathyroid hormone, alendronate, or both in men with osteoporosis. N Engl J Med 2003; **349:** 1216-26.
30. Black DM, Bilezikian JP, Ensrud KE, Greenspan SL, Palermo L, Hue T, Lang TF, McGowan JA, Rosen CJ. One year of alendronate after one year of parathyroid hormone (1-84) for osteoporosis. N Engl J Med 2005; **353:** 555-65.

31. Cosman F, Nieves J, Zion M, Woelfert L, Luckey M, Lindsay R. Daily and cyclic parathyroid hormone in women receiving alendronate. N Engl J Med 2005; **353:** 566-75.

32. Shen V, Dempster DW, Birchman R, Xu R, Lindsay R. Loss of cancellous bone mass and connectivity in ovariectomized rats can be restored by combined treatment with parathyroid hormone and estradiol. J Clin Invest 1993; **91:** 2479-87.

33. Delmas PD, Vergnaud P, Arlot ME, Pastoureau P, Meunier PJ, Nilssen MH. The anabolic effect of human PTH (1-34) on bone formation is blunted when bone resorption is inhibited by the bisphosphonate tiludronate--is activated resorption a prerequisite for the in vivo effect of PTH on formation in a remodeling system? Bone 1995; **16:** 603-10.

34. Lauritzen DB, Balena R, Shea M, Seedor JG, Markatos A, Le HM, Toolan BC, Myers ER, Rodan GA, Hayes WC. Effects of combined prostaglandin and alendronate treatment on the histomorphometry and biomechanical properties of bone in ovariectomized rats. J Bone Miner Res 1993; **8:** 871-9.

Figure(s)

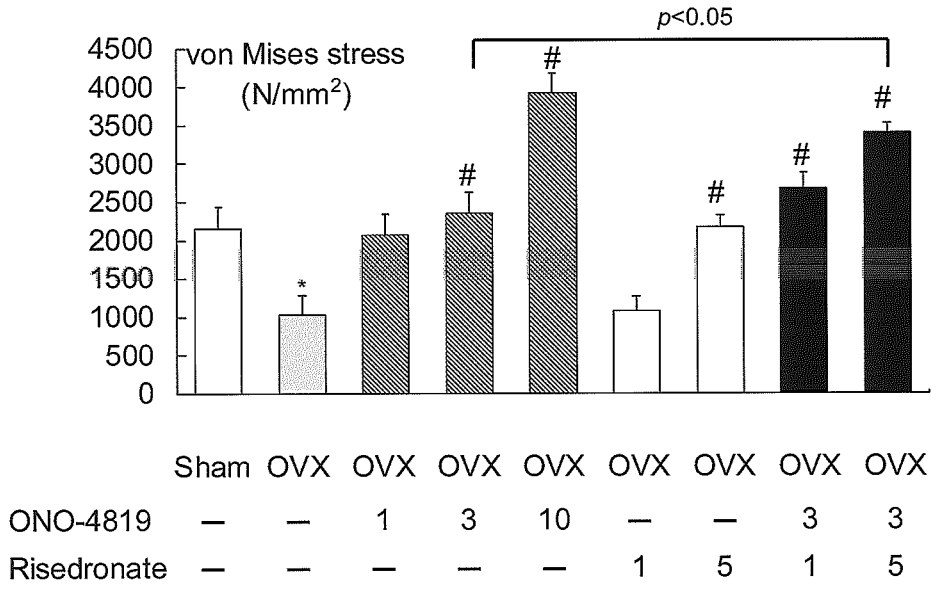

Fig.1

Figure(s)

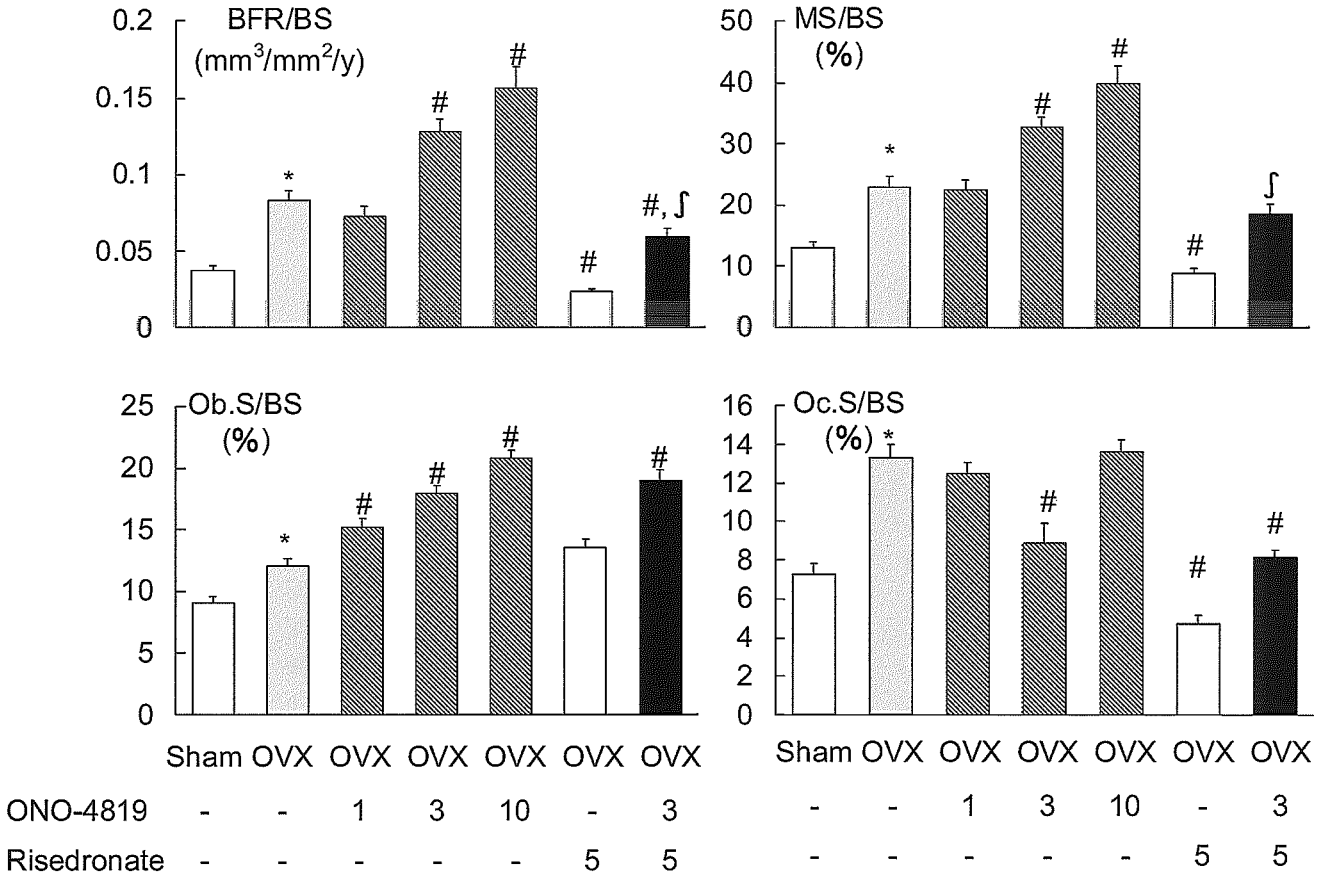

Fig.2

Figure(s)

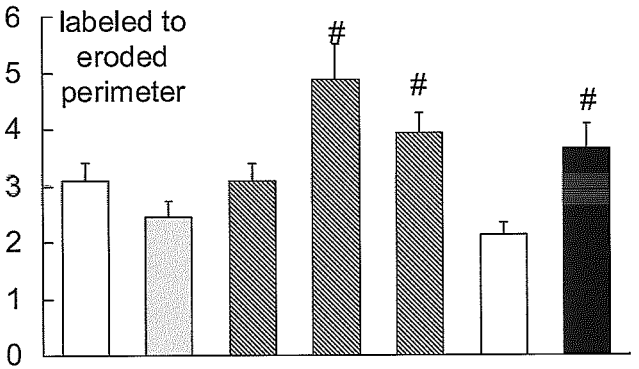

	Sham	OVX	OVX	OVX	OVX	OVX	OVX
ONO-4819	-	-	1	3	10	-	3
Risedronate	-	-	-	-	-	5	5

Fig.3

Table(s)

Table 1 Effects of ONO-4819 and risedronate on trabecular and cortical bone density in OVX rats

operation	treatment	dose	trabecular BMD	cortical density
		μg/kg BW	mg/cm^3	mg/cm^3
sham	vehicle	-	407±17	311± 9
OVX	vehicle	-	220±22 *	255±11 *
OVX	ONO-4819	1	295±120	287±12
OVX	ONO-4819	3	378±178 #	317± 7 #
OVX	ONO-4819	10	469±33 #	364±15 #
OVX	Risesronate	1	308±12 #	294± 5
OVX	Risedronate	5	346±23 #	320±12 #
OVX	ONO-4819 + Risedronat	3 + 1	393±26 #	338± 9 #
OVX	ONO-4819 + Risedronat	3 + 5	453±17 #,§	331± 7 #

33-week-old OVX rats were treated with the indicated drugs for 11 weeks. BMD of trabecular and cortical compartments at the tibiae was determined separately. Cortical density is expressed as mg/cm^3 hydroxyapatite equivalent. Data are shown as Mean±S.E. (n = 10 per group) .

*$p<0.05$ vs. sham group (by Wilcoxon runk sum test), #$p<0.05$ vs. OVX group (by Wilcoxon runk sum test), §$p<0.05$ vs. ONO-4819 (3μg/kg) alome (by Steel test)

Table(s)

Table 2 Effects of ONO-4819 and risedronate on microstructural parameters at tibiae of OVX rats

operation	treatment	dose	BV/TV	Tb.N	Tb.Th	SMI	ConnD.
		μg/kg BW		1/mm	mm		$1/mm^3$
sham	vehicle	-	0.236±0.014	3.89±0.16	0.061±0.002	1.42±0.13	94.61±9.13
OVX	vehicle	-	0.109±0.010 *	2.03±0.18 *	0.053±0.001 *	2.16±0.08 *	30.65±4.05 *
OVX	ONO-4819	1	0.160±0.014	2.70±0.17	0.059±0.002	1.83±0.10	47.82±5.03
OVX	ONO-4819	3	0.185±0.009 #	3.07±0.16 #	0.061±0.001 #	1.45±0.04 #	59.19±5.87 #
OVX	ONO-4819	10	0.315±0.023 #,†	3.86±0.23 #	0.081±0.002 #,†	0.33±0.17 #,†	69.26±7.37 #
OVX	Risesronate	1	0.140±0.011	2.73±0.15 #	0.051±0.002	2.26±0.10 †	51.94±5.29 #
OVX	Risedronate	5	0.187±0.019 #	3.22±0.20 #	0.057±0.003	1.88±0.13	71.32±6.19 #
OVX	ONO-4819 + Risedronate	3 + 1	0.228±0.021 #	3.43±0.18 #	0.066±0.003 #	1.21±0.17 #	63.86±4.92 #
OVX	ONO-4819 + Risedronate	3 + 5	0.272±0.014 #,§	3.97±0.11 #,§	0.068±0.002 #,§	1.02±0.12 #,§	89.36±3.77 #,§

33-week-old OVX rats were treated with the indicated drugs for 11 weeks. Microstructural parameters were determined by using micro CT, as described in the Methods. Data are shown as Mean±S.E.(n = 10 per group).

*$p<0.05$ vs. sham group (by Wilcoxon runk sum test), #$p<0.05$ vs. OVX group (by Wilcoxon runk sum test), †vs. sham group (by Wilcoxon runk sum test), §$p<0.05$ vs. ONO-4819 (3μg/kg) alome (by Steel test)

BV/TV: bone volume/tissue volume, Tb.N: trabecular number, Tb.Th: trabecular thickness, Tb.Sp: trabecular separation, SMI: structure model index, ConnD: connectivity density

Table(s)

Table 3 The additive effects of ONO-4819 and risedronate on BMD, bone geometry, microstructural parameters and biomechanical properties

		ONO-4819[a]	risedronate[a]	ONO-4819 + risedronate Interaction[a]	additive[b]
BMD and geometry	trabecular BMD	0.001	0.001	0.208	YES
	cortical density	0.001	0.001	0.013	NO
	cortical thickness	0.01	NS	0.439	YES
microstructural parameters	BV/TV	0.001	0.001	0.821	YES
	Tb.N	0.01	0.01	0.531	YES
	Tb.Th	0.05	0.01	0.513	YES
	Tb.Sp	0.01	0.001	0.176	YES
	SMI	0.001	0.01	0.474	YES
	ConnD	0.001	0.001	0.308	YES
	DA	NS	NS	0.882	YES
finite element analysi	von Mises stress	0.001	0.001	0.658	YES

[a]p value obtained from a two-way ANOVA analysis model on rank transformed data

[b]The effects of ONO-4819 and risedronate were considered to be additive and independent of each other if the interaction effect was not statistically significant.

BV/TV: bone volume/tissue volume, Tb.N: trabecular number, Tb.Th: trabecular thickness, Tb.Sp: trabecular separation, SMI: structure model index, ConnD: connectivity density, DA: degree of anisotropy

Resorption of auditory ossicles and hearing loss in mice lacking osteoprotegerin

Sho Kanzaki[a], Masako Ito[c], Yasunari Takada[b], Kaoru Ogawa[a], and Koichi Matsuo[b,*]

[a]Department of Otolaryngology, and [b]Department of Microbiology and Immunology, Keio University School of Medicine, 35 Shinanomachi, Shinjuku-ku, Tokyo 160-8582, Japan.

[c]Department of Radiology, Nagasaki University School of Medicine, 1-7-1 Sakamoto, 852-8501 Nagasaki, Japan.

*Corresponding author. Department of Microbiology and Immunology, School of Medicine, Keio University, 35 Shinanomachi, Shinjuku-ku, Tokyo 160-8582, Japan. Phone: +81 3 3353-1211 ext. 61223; Fax: +81 3 5360-1508.

E-mail address: matsuo@sc.itc.keio.ac.jp (K.Matsuo).

Abstract

Bones conduct sound in the middle ear. The three ossicles—the malleus, incus, and stapes—form a chain that transmits vibrations from the tympanic membrane to the oval window of the inner ear. Little is known about bone remodeling events in these ossicles, and about potential effects of osteoporosis on hearing loss. Osteoclastic bone resorption is enhanced in *Opg*$^{-/-}$ mice lacking osteoprotegerin, which is a soluble decoy receptor for the osteoclastogenic cytokine RANKL. We asked whether auditory ossicles are resorbed in *Opg*$^{-/-}$ mice, and whether these mice suffer from impaired auditory function. All three ossicles in *Opg*$^{-/-}$ mice showed thinning, especially at the malleal manubrium and incus body. Most notably, unlike in the case in wild-type mice, the junction between the stapes and the otic capsule was fixed in *Opg*$^{-/-}$ mice, and the stapedial footplate was thinner and broader. Radiological analyses revealed that malleal cortical thickness was positively correlated with tibial bone mineral density in *Opg*$^{-/-}$ and control littermate mice. Furthermore, progressive hearing loss was detected in *Opg*$^{-/-}$ mice starting at 6 to 15 weeks of age. These data suggest that osteoprotegerin plays a crucial role in hearing by protecting the auditory ossicles and otic capsule from osteoclastic bone resorption.

Introduction

The three ossicles in the middle ear, the malleus, incus, and stapes, are formed mainly by endochondral ossification of the mesenchyme from the first and second branchial arches [1, 2]. The manubrium (handle) of the malleus attaches to the tympanic membrane, while the footplate of the stapes attaches to the oval window of the cochlea. The stapedial foot is mobile and transmits vibrations to the perilymph, the fluid in the inner ear. The inner ear is contained in the otic capsule of the temporal bone, which is the hardest bone in the body.

Bone mineral density (BMD) is determined by the balance between bone resorption by osteoclasts and formation by osteoblasts. Genetic studies of osteopetrotic mice reveal a number of molecules essential for osteoclastogenesis. Osteoclasts differentiate from precursors of the monocyte-macrophage lineage in the presence of the two membrane bound cytokines, macrophage-colony stimulating factor (M-CSF) and RANKL (receptor activator of nuclear factor-κB ligand, also called osteoclast differentiation factor or TRANCE) [3]. The RANKL receptor is a tumor necrosis factor receptor superfamily member known as RANK encoded by the *Tnfrsf11A* gene. RANK signaling in osteoclast precursors activates a series of osteoclastogenic transcription factors including NF-κB, c-Fos/AP-1, and NFATc1 [4-9]. The osteoclastogenic activity of RANKL is masked by the soluble decoy receptor osteoprotegerin (OPG, also called osteoclast inhibitory factor), encoded by *Tnfrsf11B* [10, 11]. In bone remodeling, BMD is maintained by a coupling of osteoclastic bone resorption with subsequent osteoblastic formation [12].

In human populations, the incidence of osteoporotic hip fracture increases

exponentially with age [13]. Age-related hearing loss, or presbycusis, affects more than one third of individuals above the age of 75 [14]. Although a link between osteoporosis and hearing loss has been suggested [15-17], recent epidemiological studies reveal no correlation of hearing loss and osteoporosis in elderly women [18], a finding that seems counterintuitive given that hearing largely depends on bone.

Opg$^{-/-}$ mice develop osteopenia due to enhanced differentiation of osteoclasts [19-22]. To gain deeper insight into the role of bone remodeling in hearing, we asked if auditory ossicles are susceptible to osteoclastic bone resorption in *Opg*$^{-/-}$ mice and whether auditory function is impaired.

Materials and methods

Mice

Female *Opg*$^{-/-}$ and heterozygous control mice on a C57BL6 background were purchased from Clea Japan. All experiments were conducted in accordance with institutional review board-approved protocols.

Morphological analyses

Mouse skulls were fixed in 4% paraformaldehyde. For macroscopic analysis, auditory ossicles were isolated by removing the temporal bone, stained for tartrate-resistant acid phosphatase (TRAP) activity using the Leukocyte Acid Phosphatase Kit (Sigma), and observed using a SMZ1500, stereoscopic zoom microscope configured with the Eclipse 90i digital camera system (Nikon). For histological analysis, skulls were decalcified in 0.5 M EDTA for one week, and the temporal bones containing auditory ossicles were trimmed and embedded in paraffin. Frontal sections of 5 μm thickness were stained with HE and for TRAP activity.

Radiographical analyses

Each isolated malleus was embedded in melted 8% gelatin in a segment of a plastic drinking straw. After solidifying the gelatin at 4°C, mallei were scanned using micro-computed tomography (μCT) instrumentation (μCT-40, Scanco Medical AG, Switzerland). Based on two-dimensional data from scanned slices, cortical thickness was calculated by setting the volume of interest (VOI) to the entire malleus. Tibial cortical BMD was measured using a CT scanner (LaTheta LCT-100, Aloka, Japan) with isolated bilateral tibiae.

Auditory brain-stem response (ABR) measurement

A needle electrode was subdermally inserted at the vertex along the dorsal midline of the scalp between the external auditory canals. The reference electrode was placed below the pinna of the left ear, and the ground electrode was inserted below the contralateral ear. The sound stimulus consisted of a 1 ms tone burst with a rise-fall time of 0.1 ms. For each stimulus, ABR waveforms were recorded for 12.8 ms at a sampling rate of 40,000 Hz using 50-5000 Hz bandpass filter settings, and waveforms from 256 stimuli at a frequency of 9 Hz were averaged. ABR waveforms were recorded in 5-dB sound pressure level (SPL) intervals down from a maximum amplitude until no waveform could be observed using Scope software of the PowerLab system (PowerLab2/20, AD Instruments, Australia). ABRs were performed on mice aged 6, 10, and 15 weeks at the following frequencies: 2, 4, 12, and 20 kHz. ABRs were measured under anesthesia induced by intraperitoneal injection of 0.01 ml/g body weight of 2.5% avertin. The researcher who measured ABRs was unaware of the identities of the animals.

Statistical analysis

Statistical comparisons were performed using Student's *t*-test and analysis of variance, where appropriate.

Results

To examine the morphology of the auditory ossicles in *Opg*$^{-/-}$ mice, we isolated mallei, incudes and stapes from the middle ear cavities of 10-week-old *Opg*$^{-/-}$ mice and from wild-type and heterozygous controls. We observed that the junction between the stapes and the oval window of the cochlea was tighter in *Opg*$^{-/-}$ mice compared to control mice. Ossicles from *Opg*$^{-/-}$ and control mice were stained for TRAP activity, which is a marker for osteoclasts and resorption lacunae. Compared to wild-type and heterozygous controls, all three ossicles in *Opg*$^{-/-}$ mice were more heavily stained for TRAP activity and exhibited thinning, particularly at the malleal manubrium, malleal processus brevis, incus body, and stapedial arch (Fig. 1a). Furthermore, the stapedial footplate was thinner and broader at the periphery in *Opg*$^{-/-}$ mice (Fig. 1a, Stapes, top view). Such thinner parts of ossicles, especially of the stapes, exhibited intense TRAP staining (Fig. 1a).

To further analyze osteoclasts in the auditory ossicles, histological sections of the temporal bone from wild-type, heterozygous, and *Opg*$^{-/-}$ mice were stained for TRAP activity. Compared to wild-type and heterozygous controls, TRAP-staining was much stronger in both auditory ossicles and the otic capsule in *Opg*$^{-/-}$ mice (Fig. 1b and data not shown). We next quantitated the number of TRAP-positive multinucleated cells (MNCs) in wild-type, heterozygous and *Opg*$^{-/-}$ mice (Fig. 1c). The number of TRAP-positive MNCs was significantly higher in *Opg*$^{-/-}$ mice than in controls, suggesting that osteoclastic bone resorption of auditory ossicles is dramatically enhanced in *Opg*$^{-/-}$ mice.

We also histologically examined the junction between the stapes and the otic capsule in heterozygous and *Opg*$^{-/-}$ mice. The ligament between the stapedial footplate

and otic capsule was intact in heterozygous mice (Fig. 2a), while no ligament was seen in *Opg*$^{-/-}$ mice, and the junction was replaced with bone tissue fusing the stapes and otic capsule (Fig. 2b).

We next examined the auditory ossicles radiographically. Imaging using μCT of isolated mallei confirmed massive erosion in ossicles of *Opg*$^{-/-}$ mice, which was not observed in heterozygous mice (Fig. 3a). Based on the μCT images, cortical thickness of mallei was calculated in *Opg*$^{-/-}$ mice and controls. Malleal cortical thickness observed in *Opg*$^{-/-}$ mice was significantly lower than that seen in heterozygous controls (Fig.3b). As expected, tibial cortical BMD of *Opg*$^{-/-}$ mice was also lower than that seen in heterozygous mice (Fig. 3c). Consistent with the histological data, these data suggest that osteoclastic bone resorption of auditory ossicles is elevated in the absence of OPG, leading to bone loss.

To test whether bone loss observed in *Opg*$^{-/-}$ mice is associated with differences in hearing ability, we assessed ABR thresholds at 6, 10 and 15 weeks of age in heterozygous and *Opg*$^{-/-}$ mice. ABR threshold was determined as the minimum sound pressure level (SPL) giving reproducible waveforms. At 6 weeks of age, the average ABR threshold of *Opg*$^{-/-}$ mice was similar to that of heterozygous littermate controls at frequencies from 2 to 20 kHz. However at 10 weeks of age, *Opg*$^{-/-}$ mice began showing higher (i.e., worse) thresholds than controls (Fig. 4). By 15 weeks, the differences were even greater, with *Opg*$^{-/-}$ mice being more than 20 decibels (dB) less sensitive than heterozygous controls at the highest frequency of 20 kHz (Fig. 4). These data suggest that excessive bone remodeling can result in progressive hearing loss.